National College of Ireland

Liver Tumour Segmentation Using Deep Learning

MSc Research Project
Data Analytics

ALBIN BABY
Student ID: x23173742

School of Computing
National College of Ireland

Supervisor: Mr. Hicham Rifai

National College of Ireland

MSc Project Submission Sheet

School of Computing

Student Name: ALBIN BABY

Student ID: x23173742

Programme: Data Analytics **Year:** 2024

Module: MSc Research Project

Supervisor: Mr. Hicham Rifai

Submission Due Date: 12-12-2024

Project Title: Liver Tumour Segmentation Using Deep Learning

Word Count: 7699 **Page Count:** 30

I hereby certify that the information contained in this (my submission) is information pertaining to research I conducted for this project. All information other than my own contribution will be fully referenced and listed in the relevant bibliography section at the rear of the project.
ALL internet material must be referenced in the bibliography section. Students are required to use the Referencing Standard specified in the report template. To use other author's written or electronic work is illegal (plagiarism) and may result in disciplinary action.

Signature: ALBIN BABY

Date: 12-12-2024

PLEASE READ THE FOLLOWING INSTRUCTIONS AND CHECKLIST

Attach a completed copy of this sheet to each project (including multiple copies)	□
Attach a Moodle submission receipt of the online project submission, to each project (including multiple copies).	□
You must ensure that you retain a HARD COPY of the project, both for your own reference and in case a project is lost or mislaid. It is not sufficient to keep a copy on computer.	□

Assignments that are submitted to the Programme Coordinator Office must be placed into the assignment box located outside the office.

Office Use Only	
Signature:	
Date:	
Penalty Applied (if applicable):	

Liver Tumour Segmentation Using Deep Learning

Abstract

This study focuses on improving the liver tumour segmentation by using state-of-art deep learning architectures including U-Net and V-Net integrated with residual networks such as ResNet and Inception. The study addresses the challenge of in methods used in medical image analysis particularly the detection of tumours is computationally expensive and is inaccurate. Transfer learning and a hybrid of loss functions (focal loss, Dice loss) increase computational efficiency to improve segmentation time from minutes to milliseconds, the results of empirical testing indicate an improvement of accuracy and the decrease of computational time of the model, based on such criteria as precision and recall, as well as the F1-score. These attributes have important clinical advantages as they accelerate and improve the accuracy of the diagnosis and location of liver tumours.

Keywords: Liver tumour segmentation, Medical Imaging, TensorFlow, Deep Learning, CNN

1. Introduction

1.1 Background

The need for efficient analysis of medical images has boosted the development of Human-Computer Interaction (HCI) technologies and mainly in classifying and segmenting images of the medical variety such as MRI and CT scans (Rahman *et al.* 2022). Both radiologists and oncologists may spend hours in doing tumour staging of such diseases as liver cancer, which is one of the most fatal illnesses in the world. Conventional approaches to tumour detection are often slow and may also present a high level of variability. These inefficiencies can be lowered by using automated segmentation techniques, where deep learning is applied. Other CNN-based architectures such as, V-Net and U-Net have been useful in handling the 3D medical image data. These models yield improved segmentation accuracy but the pronounced problem in terms of computational time efficiency and V-Net is slightly superior compared to U-Net but fails to create dense feature maps (Du *et al.* 2020). The possibility of integrating deep Residual networks like ResNet and Inception with segmentation structures can improve the recognition of liver tumours.

The relevance of this work is the expanded potential to improve the techniques of liver tumour identification and segmentation, which play a significant role in the care of patients by radiologists and oncologists. The present work aims at enhancing the general accuracy of segmentation and overcoming the existing challenges of computationally costly models via the use of transfer learning and pretrained

deep learning architectures like U-Net, V-Net, ResNet, and Inception. Fine refining the model using transfer learning, together with hybrid loss functions (focal loss function, Dice loss) boosts the capacity and lower the detection time from minutes to milliseconds.

This research proposes to make use of these enhanced models in tumour segmentation while addressing the computational challenges. This can be achieved through the use of transfer learning and attempting to use the hybrid loss functions (focal loss, Dice loss) that minimizes the time needed for the tumour detection enhancing the speed of the prognosis and making it clinically relevant.

1.2 Research Question

- How the U-Net, ResNet, and V-Net architectures compare in terms of performance for liver tumour segmentation in CT images?

1.3 Research Objectives

- To develop a precise liver tumour segmentation model using U-Net, ResNet, and V-Net architectures for enhanced diagnostic accuracy
- To evaluate the effectiveness of quantitative methods in improving the accuracy of liver tumour segmentation
- To validate the use of secondary data from Kaggle for liver tumour segmentation analysis in medical imaging research

1.4 Report Structure

Introduction, section presents the significance of AI in the segmentation of liver tumours and includes the research questions and objectives based on secondary data and Python software. Literature Review present issues such as the variability of tumour shapes and the limitations that stem from existing means of segmentation that this research addresses. Research Methodology explains the quantitative approach, in this case, the identified secondary data from Kaggle which will be analysed under Python 3.11.4. because of the advantage in automating and boosting the accuracy of segmentation. Implementation explains the process of applying this AI algorithm with Kaggle datasets entailing challenges such as overfitting in building, training, and improving this model. Discussion and Conclusion provide a succinct description of the research investigations, limitations applied, and references to future research endeavours focused on segmentation improvement and model applicability to clinical settings.

2. Literature Review

2.1 Introduction

These studies have used quantitative techniques to improve the accuracy of the liver tumour boundary delineation describing concerns such as model reliability, and segmentation reliability in the context of clinical application.

In this chapter, deficiencies and issues with previous studies are described to justify the requirement for improved liver tumour segmentation techniques (Amin *et al.* 2022). A literature review of the prior work and techniques shows the benefits of the project to the improvement of the diagnostic performance in liver tumour diagnosis by employing machine learning segmentation.

2.2 Literature Study

Conducted at the Post Graduate Institute of Medical Education and Research Hospital in Chandigarh, India, and including 120 patients, the study categorises patients in terms of liver function, with 58 patients in grade A and 62 in grade B (Liu *et al.* 2021). This paper presents an AI technique using the K-means clustering algorithm for liver tumour segmentation and analyses its performance with the deep learning approach. The experiment showed that liver tumours in plain CT appear as low density and had moderate enhancement in the arterial phase and low-density nodules in blood vessels in PVP.

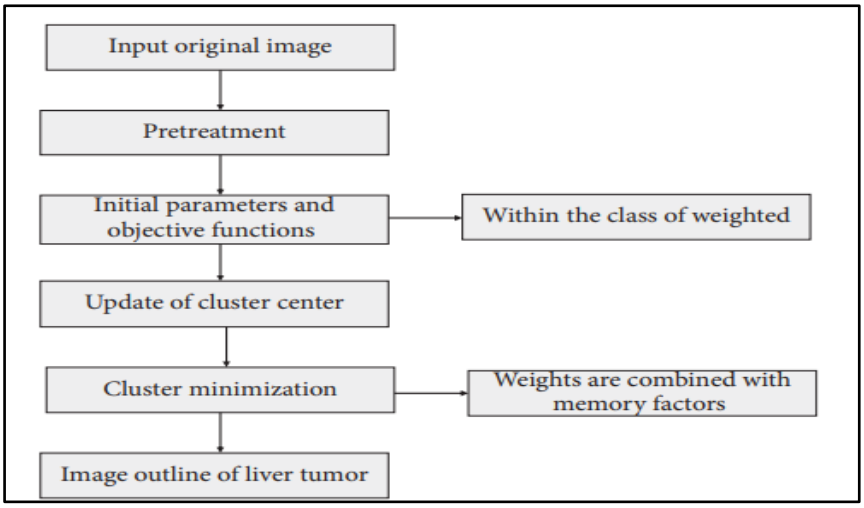

Figure 2.1: The flow chart of the KMC algorithm *(Source: Liu et al. 2021)*

The actual flowchart of the KMC algorithm demonstrates a chronological arrangement of processes that help to isolate liver tumour outlines from images. There are five different steps in the TPCPS: input of the original image, image pretreatment, determination of initial parameters and objective functions, cluster updating and minimization, combination of weights with memory factors and the production of the final image outline. The significance of this study was that CT scans proved to have

higher sensitivity than specificity in identifying liver metastasis compared to HCC (P <0.05). This has also emerged that LCT has a significant deposition impact, La patients with rich blood type yield 53.14% good deposition while 25.73% of poor blood type patients demonstrated poor deposition (Liu *et al.* 2021). The KMC algorithm is superior to the RG method and provides better treatment for segmentation results of liver tumours. These results generalise the applicability of the KMC algorithm as a tool for improving liver tumour detection and treatment planning in medical imaging.

Hu et al (Hu *et al.*, 2023) Provides a new method of liver tumour segmentation based on AI that helps avoid the use of manual annotations on CT scans. In order to train the machine to detect and segment liver tumours, synthetic tumours are created with an appearance and texture close to that of the actual ones. The synthetic tumours look realistic in such a way that they were able to pass what authors called the Visual Turing Test with pathologists failing to distinguish the synthetic models from actual ones (Hu *et al.*, 2023). This method uses clinical expertise and complex signal processing algorithms to encode such critical features as the position, morphology and texture of the tumour into the synthetic data. Since this obviates the need for highly accurate manual annotations for guiding the deep learning algorithm, it greatly lowers the cost and time required for the development of medical imaging AI systems.

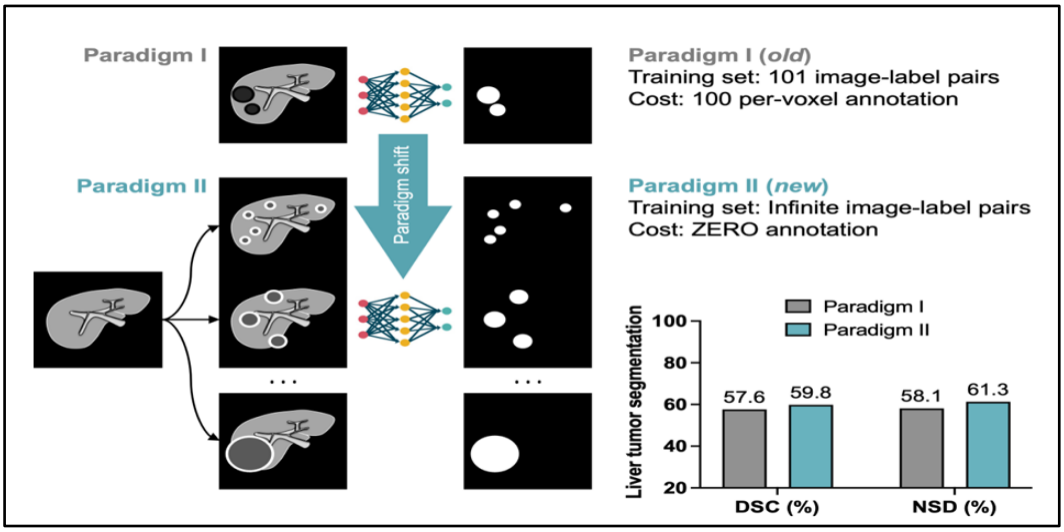

Figure 2.2: The paradigm shift from label-intensive to label-free tumour segmentation *(Source: Hu et al. 2023)*

The following image shows two paradigms for liver tumour segmentation. Paradigm I features a small set of one hundred examples with high costs inherent in the annotation process, whereas Paradigm II includes potentially a vast number of examples limitless in number with a zero cost of annotation. The image also illustrates that Paradigm II offers segmentation performance that may be higher than or similar to Paradigm I even though the former is based on zero-cost annotation, presenting the case for a shift in a medical image analysis paradigm. The results show that the AI models trained on synthetic tumours are at least as effective and, in most cases, much better than the models trained on the real

tumours with the annotations done manually. This approach also presents a higher sensitivity for detecting small tumours, which is critical for cancer diagnosis at the early stage (Hu *et al.* 2023). The synthetic Tumour generation process enables evaluation of the model perturbation with various types of Tumours since the variations are generated. This work opens the door to developing more scalable approaches to implementing AI for the visualisation of medical images in general as well as for detecting liver tumours and segmenting them based on a label-free approach.

Artificial Intelligence in Medical

The modern development in artificial intelligence has helped improve medical image, most notably ultrasonography or the US. Safely, malignant lesions may be missed by mistake or intentionally in the US resulting in dangerous health complications; AI provides a plausible input to this by minimising human mistakes. It has been established that utilising AI for medical imaging is reliant on numerous factors inclusive of the imaging modality, suitable datasets, relevance of the chosen algorithm, together with expected clinical outcomes. Together with the US, AI-powered radiomics is also seen as a potential approach to develop HCC outcomes prediction and more tailored interventions as well.

Liver cancer is a leading global health problem, especially for accurate identification and targeting of liver tissue and tumours since the problem of accurate segmentation partly contributes to poor diagnosis and treatment. MRI, CT and ultrasound scans are the typical functional imaging approaches utilised while diagnosing Liver tumours but these come with challenges of similar signal intensity of the tissues and variable shape and position of the organ (Rahman *et al.* 2022). These challenges make conventional segmentation techniques suppressing the possibility of isolating liver tumours in CT scans to black and white or based on shape very ineffective. These limitations are mitigated in this study by developing a novel ResUNet model that integrates both ResNet and UNet structures to improve the precision and speed in the liver and tumour segmentation in CT image volumes.

2.3 Theoretical Framework

The foundation of AI-driven analysis for liver tumour segmentation is based in the furtherance of medical images and artificial neural networks. The difficulties of liver tumour segmentation stem from the internal structure of the liver, overlapping opacities and irregular tumour margins (Qiu *et al.* 2024). Techniques such as MRI, CT and ultrasound scans by themselves fail to offer the desired degree of segmentation accuracy and this is why an AI-based solution is the only viable remedy so far as detection efficacy is concerned. Segmentation AI frameworks such as K-means clustering ResUNet and synthetic tumour generation for dependable segmentation use deep learning.

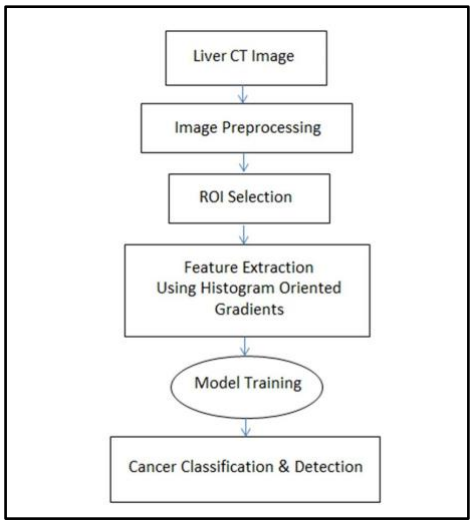

Figure 2.3: Conceptual Model of Liver Tumour Segmentation *(Source: Chierici et al. 2020)*

According to the discussion, ResUNet integrates feature extraction from ResNet and segmentation from UNet, while data syntheses minimise reliance on annotated tumour replicas. K-means clustering and label-free models show that AI can be used to segment liver tumours with little specialist labelling, which saves money (Chierici *et al.* 2020). These frameworks make use of AI in conjunction with certain imaging techniques such as CT scans and ultrasound, for early diagnosis, precise tumour delineation as well as technological and clinical needs for managing liver cancer.

2.4 Literature Gap

There are still some gaps that have been found in the literature concerning the developments in AI for liver tumour segmentation. Thus, while multiple works show high accuracy of the segmentation results using UNet + ResNet and K-means clustering, most works employ clean artificial datasets with less variability in the capturing parameters. This is a limitation that we find in real-world applications since AI models may fail to perform well when exposed to highly heterogeneous clinical imaging data, especially in ultrasound where the relative variability of image quality due to patient attributes and machine settings affects the system quite significantly (Fallahpoor *et al.* 2024). Limited investigations have simultaneously investigated the ability of AI models with different imaging environments, the assessment of which is essential for widespread implementation.

2.6 Critical Assessment

Despite the proportionate progress in liver tumour segmentation based on AI, some aspects remain largely compelling and may affect its real-world applicability. Algorithms such as UNet+ResNet and K-means clustering appear to have considerable segmentation precision, but most tests are conducted on carefully selected test suits with little variation. This concentrating on the one hand on data

incorporating perfect image information disregards the variations most likely to prevail in real clinical practice scenarios, especially in ultrasound imaging where due to variability in patient's anatomy also variability in settings of an imaging machine high heterogeneity is most probable (Saha Roy *et al.* 2023). Most of the existing AI models do not have the stability that enables them to work well across different imaging scenes, hence questioning their applicability.

Though synthetic data generation provides an innovative way of addressing the expensive venture of manual annotation, it is still a relatively young technology. Present synthetic tumour models, while performing reasonably well in supervised tests, fail to mimic actual tumour characteristics, fine texture and density. This gap raises the understanding of the current literature by stressing the further necessity of validation studies to test synthetic data efficiency in training AI models for clinical applications (Bakrania *et al*. 2023). It is rather rare to find research that provides a general overview of synthesised data-trained models and benchmarks them against those trained using annotated real datasets. All of these limitations with a broad range of data and sophisticated synthetic approaches can make the AI segmentation tools more flexible, accurate, and ultimately more useful in the liver cancer field.

3. Research Methodology

3.1 Introduction

This chapter focuses on explaining the strategies used in conducting this research, such as an effective and precise liver tumour segmentation model that is achieved using the selected architectures, including U-Net, ResNet, and V-Net. The use of those methodologies sought to improve the diagnostic outcomes and meet the ethical practice in the processing of medical imaging data.

3.2 Research philosophy

The study met a positivist epistemology, doing away with subjectivity, the study embracing empirical evidence and scientific validity. Positivism is based on the assumption that knowledge is the function of observable and measurable data, and as a result, it is appropriate to use it exclusively in quantitative research like the present study. Using this philosophy, the study aimed at trivializing consequences, replicating procedures, and showcasing standard methods and statistical reliability.

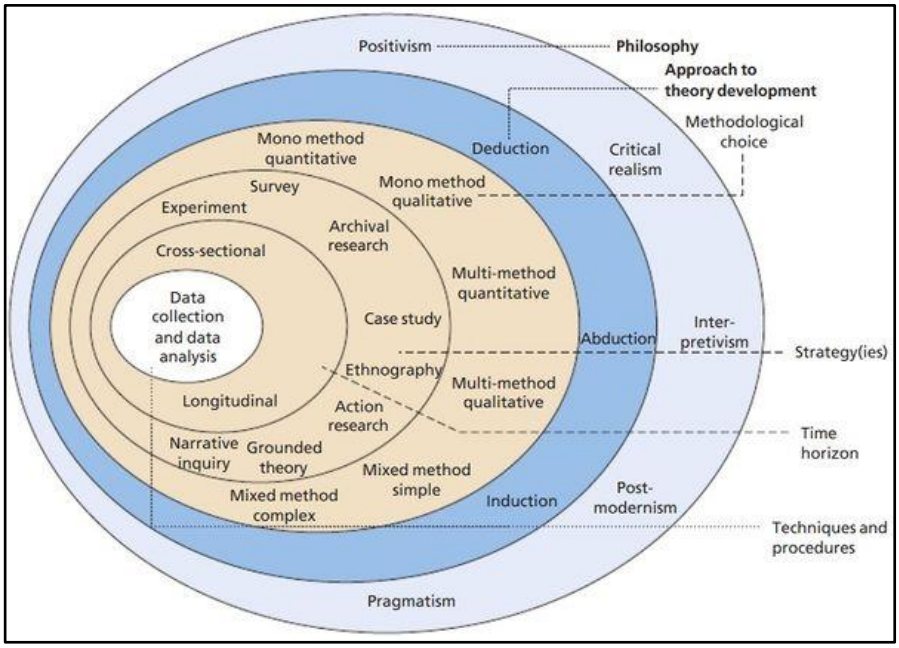

Figure 3.1: Research philosophy (Source: Lewinson, 2020)

This also helped to prevent a bias in the study because the data collected has been quantifiable and obtained from secondary sources. Continuing this approach has been simple, as U-Net, ResNet, and V-Net models could be easily quantified and their performance has been empirically measurable.

3.3 Research Approach

The study used both an exploratory research approach and a confirmatory research approach as well as the positivist research philosophy and quantitative research method. This approach started with developing hypotheses grounded on the hypothetical and previous studies on liver tumour segmentation and medical image analysis. The study proceeded to validate these hypotheses and employed advanced segmentation models of U-Net, ResNet, and V-Net using Kaggle real, reliable, and large datasets. The deductive approach provided for a systemized procedure of research as the results obtained would be definitively quantifiable and assessed in terms of set benchmarks.

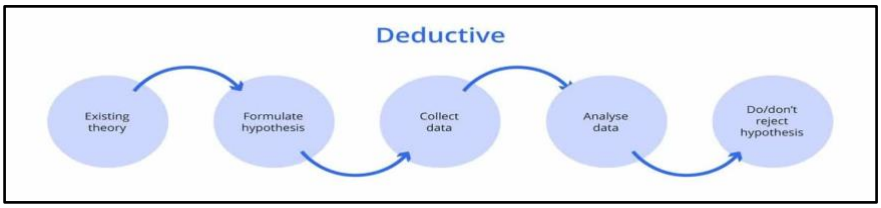

Figure 3.2: Process of Deductive Approach *(Source: Nahrstedt et al. 2024)*

This approach had several advantages, such as the clear identification of the structure of the study and the use of hypotheses to make specific conclusions. The deductive strategy improved the accuracy and credibility of the results due to following pre-existing paradigms and quantitative techniques (Nahrstedt *et al.* 2024).

3.5 Data collection method

The technique of data collection for this particular research has been secondary data, which has been obtained from the Kaggle website. This dataset gave a good benchmark to compare different methods used in the segmentation of advanced liver tumours, including U-Net, ResNet and V-Net. Secondary data has been selected because it has been easily available, pertinent, and collected in a format that eliminates nearly all the time and effort in the data accumulation process (Farrens *et al.* 2020).

3.6 Data Acquisition

The dataset is acquired from a secondary data sources listed. The dataset used in this work was obtained from Kaggle.com and includes images of labelled patients who have been imaged at different clinical centres across the globe. It has its origin in the LiTS (Liver Tumour Segmentation, sample image is showcased in the Figure 3.3 LiTS sample images) Challenge held during ISBI 2017 and MICCAI 2017 and offers an enhanced dataset to use and improve studies in the fields of medical image analysis and segmentation.

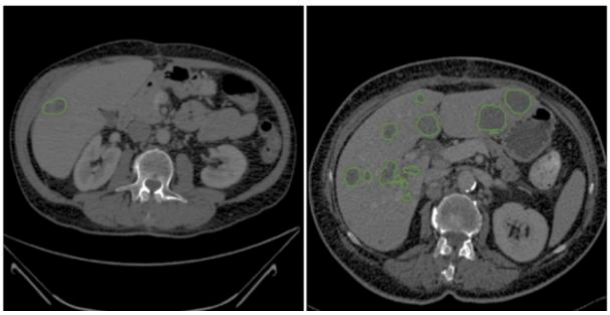

Figure 3.3 LiTS sample images

The dataset is collated across various geographical institution to enhance the demographic collection detail and the utility of it. The Figure 1 Distribution Sample of the Universities towards LiTS dataset showcases the visual representation of the data distribution in the Liver Tumour Segmentation dataset.

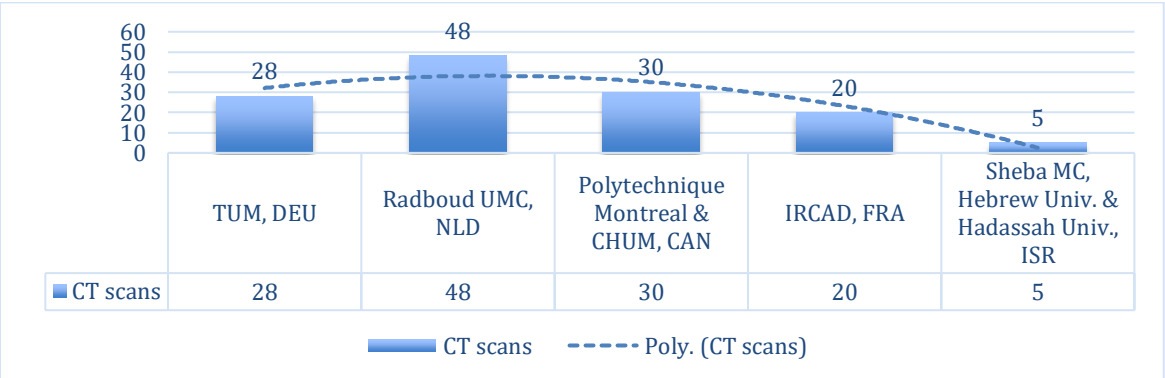

Figure 1 Distribution Sample of the Universities towards LiTS dataset

3.7 Data Preprocessing and Transformation

3.7.1 Data Loading and Description

The dataset contains four columns, directory name or the directory name, filename, mask filename and mask directory name. The columns are defined on the Table 1 Data Availability

Table 1 Data Availability

Column Name	***Description***
dirname	Directory path to the folder containing the input CT scan volume files.
filename	File name of the CT scan volume.
mask_dirname	Directory path to the folder containing the segmentation mask files.
mask_filename	File name of the segmentation mask corresponding to the CT scan volume.

3.7.2 Image Preprocessing

Normalisation

The normalisation framework allows the image dataset, to be reduced within pixels of 0 and 1. This further nuance the need to prevent overfitting as well as the reduction of data channels to reduce computation. To achieve normalisation there are multiple techniques and methods, the paper uses mean-based normalisation as showcased by the Equation 1

$$\delta_{normalised} = \frac{(\delta - \mu)}{\sigma}$$

Equation 1

Bilateral Filtering

The liver CT scan although is an artificially created image but due to the presence of human error, mechanical noise and instrumental differentiation across various university and hospitals involved the dataset is catered with the presence of noise unanimously across many samples. To prevent this the paper introduces the use of bilateral filtering to avoid noise within the images. The bilateral filtering uses the spatial and radial kernel across each pixel where in W_s for spatial kernel, W_r for radial and $\Delta_{a,b}$ representing all pixels within the range of 0 to 256 noted by a, b.

$$Bilateral\ Filtering\ (I)(\Delta_{x,y}) = \left(\frac{1}{W_{xy}}\right) \sum_{(a,b)\in N_{ab}}^{N_{ab}} I(\Delta_{a,b})\ .\ W_s\left(\Delta_{a,b}, \Delta_{x,y}\right).W_r(\Delta_{a,b}, \Delta_{x,y})$$

Equation 2

Equation 2 describes the bilateral filtering operation on image $I(\Delta_{a,b})$ and Equation 3 and Equation 4 describe the spatial and radial kernels for noise filtration

$$W_s\ \left(\Delta_{a,b}, \Delta_{x,y}\right)\ or\ Spatial\ kernel = \ e^{\frac{(-||\ \Delta_{a,b}, \Delta_{x,y}\ ||^2\ )}{2\sigma_s}}$$

Equation 3

$$W_r\ \left(\Delta_{a,b}, \Delta_{x,y}\right)\ or\ Radial\ kernel = \ e^{\frac{(-||\ \Delta_{a,b}, \Delta_{x,y}\ ||^2\ )}{2\sigma_r}}$$

Equation 4

The sample output of the image as a focus of bilateral filtering and normalisation is showcased by Figure 2 Liver Tumour Data after Bilateral Filtering and Normalistion.

Figure 2 Liver Tumour Data after Bilateral Filtering and Normalistion

Encoding

The mask output is adjusted to either 0 and 1 for categorical cross-entropy calculation, thus encoding helps in adjusting the levels of background and adjusting tumour pixels. Its further showcased in the Equation 5.

$$OP\ = \begin{cases} 0, & x < 0 \\ 1, & x\ > 0 \end{cases}$$

Equation 5

3.8 Modelling UNET and Transfer Learning techniques (UNET-TLT)

The study proposed the implementation of UNET with Resent transfer learning approach, Unet consists of the encoder, decoder and bottleneck subsections. To have a detailed purview of the model the architecture diagram is showcased in Figure 3 UNET Architecture Diagram.

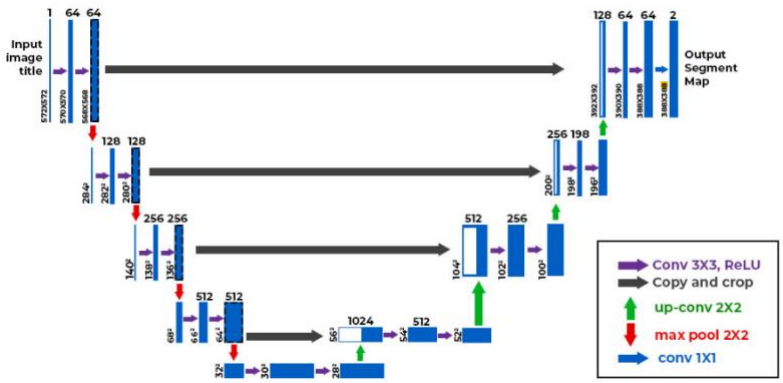

Figure 3 UNET Architecture Diagram

Figure 3 UNET Architecture Diagram illustrates the input and output shape transitions within the UNET architecture simulation, using convolutional neural network, Batch Normalization, Leaky RELU for activation unit, Max Pooling 2D to reduce the feature filtering to important pixel within the 2x2 window, Dropout to prevent overfitting, Up Sampling 2D for recreation of the mask image, Concatenate, and SoftMax for the final mask prediction.

Transfer Learning technique Residual neural network

The residual neural network which is used in simulation to the UNET allows for high level feature extraction as well as the reduction of gradients in case of exploding gradient. Also because of vanishing gradient the weight upgrade defined by the Equation 6; this happens as $\nabla_w L(w_t)$ which is the loss with respect to the w_t i.e. the weight in time t gets to zero and no further weight changes takes place.

$$[w_{t+1} = w_t - \eta \nabla_w L(w_t)]$$

Equation 6

To prevent this gradient flow stimulus the UNET architecture uses RESNET with the creation of an auxiliary layer unit using the concatenation function and to allow more gradients to reach the weights without becoming 0.

Loss Function for UNET-TLT

The loss function for the UNET-TLT is a joint hybrid weighted function given by the Equation 7 where the dice loss is described by Equation 8 and focal loss by Equation 9.

$$\text{Total Loss} = 0.8 \cdot \text{Dice Loss} + 0.2 \cdot \text{Focal Loss}$$

Equation 7

Equation 8 defines Dice Loss which is a metric used to measure the overlap between two samples

$$\text{Dice Loss} = 1 - \frac{2\sum_i y_i \widehat{y_i}}{\sum_i y_i + \sum_i \widehat{y_i}}$$

Equation 8

Equation 9 defines the Focal Loss which is designed to address class imbalance by down-weighting (with hyperparameter α_c) the loss assigned to well-classified examples

$$\text{Categorical Focal Loss} = -\sum_{c=1}^{C} \alpha_c (1 - \widehat{y_c})^{\gamma} \log(\widehat{y_c})$$

Equation 9

In Equation 8 and Equation 9 $\widehat{y}$ defines the predicted vectors and y defines the actual ground truth.

Hyperparameter for UNET-TLT

Table 2 Hyperparameter table for UNET-TLT

Hyperparameter	Description
Input Image Size	256x256
Number of Filters	128 and 256
Kernel Size	5x5
Stride	2
Padding	SAME
Activation Function	ReLU, LeakyReLU, Softmax
Batch Normalization	YES
Dropout Rate	0.2
Optimizer	ADAM
Learning Rate	0.0001
Loss Function	Given by hybrid loss function in Equation 7
Number of Epochs	200
Batch Size	8
Number of Classes	2

3.8 Summary

In the methodology chapter, a well-coordinated procedure to create and assess state-of-the-art liver tumour segmentation models using U-Net, ResNet, and V-Net models has been clearly explained. The deductive research approach has been also selected, which is directed to develop hypotheses of interactions between several factors. Data collected from Kaggle has been secondary data which has been particularly efficient and has been anonymized to meet the strict ethical requirements. The quantitative measures allowed for the accurate measurement of the model performances which helped in using a differential diagnosis tool.

4. Design and Implementation Specifications

Data Preparation

The dataset is divided into training (70%), testing (20%), and validation (10%) sets, as showcased by Table 3 Dataset training, testing and validation splits,for utility of the segmentation model. The training set of 91 images of the liver lesion. The testing set of 26 images of unseen data. The validation set of 13 images for fine-tuning the model and prevent overfitting.

Table 3 Dataset training, testing and validation splits

DATASET SPLIT	NUMBER OF CT SCANS	PERCENTAGE
TRAINING	91	70%
TESTING	26	20%
VALIDATION	13	10%

The dataset is loaded with python pandas module and applied with three preprocessing techniques namely normalisation, bilateral filtering and adjusted encoding for the mask of the tumor image. The normalisation techniques allow the image to be grayscaled and encoding allows 0 and 1 values only to be present in the mask. This helps in reducing any noise in the optimisation scale and loss calculation.

UNET-TLT

The Unet transfer learning techniques as illustrated in the above section also consists of primarily three segments of implementation, namely the forward propagation, backward propagation and optimisation.

Forward Propagation

The forward propagation is an essential aspect of the neural network, the UNET-TLT uses the forward propagation to calibrate the randomised weightage matrix for the delineation and creation of the features. Generally, in the calibration of forward propagation l defines the current layer wherein ‘i’ and ‘j’ is the weight notation. Equation 10 showcases the weighted calculation of the output vector z, where in a is the input vector, b is the biases, and w defines the weight matrix for the layer l

$$z_j^{(l+1)} = \sum_i \left(w_{ij}^{(l)} \cdot a_i^{(l)} \right) + b_j^{(l)}$$

Equation 10

Equation 11 defines the activation unit, the activation unit is responsible for introducing non linearity within the neural network. This is essential as it allows the neural network to fire on cases of the specific input simulation, allowing for feature selection and feature extraction. f defines the function of activation.

$$a_j^{(l+1)} = f\left(z_j^{(l+1)}\right)$$

Equation 11

There are multiple activation function which are used in the UNET-TLT method namely, RELU, Sigmoid, SoftMax and LeakyRelu. Equation 12 defines the ReLU activation function which negates the negative vectors to 0 and allow only the positive simulation to reach the next neuron. This creates an auxiliary neuron firing scenario in case of input variable change as showcased by the Figure 5 Sigmoid Graph.

$$\text{ReLU}(z) = \max(0, z)$$

Equation 12

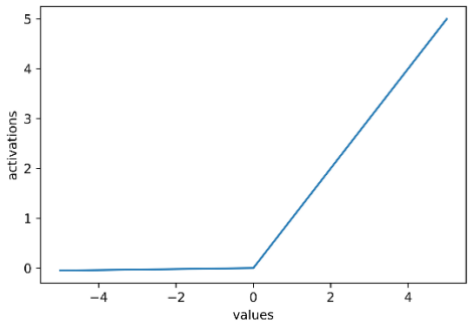

Figure 4 ReLU activation Unit

Equation 13 defines the sigmoid function where in z is the input from the weighted equation. The showcased by the graph in Figure 5 Sigmoid Graph.

$$\text{Sigmoid}(z) = \frac{1}{1 + e^{-z}}$$

Equation 13

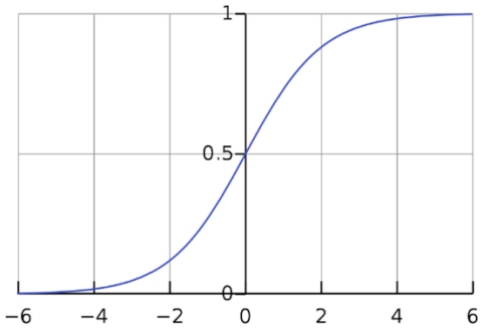

Figure 5 Sigmoid Graph

Equation 14 defines the SoftMax function which is used in the last layer of the masking unit allowing for the probability distribution of each neuron. This firing precision is needed for classification of pixels into 0 or 1 meaning background or tumour

$$\text{SoftMax}(z_i) = \frac{e^{z_i}}{\sum_j e^{z_j}}$$

Equation 14

Backward Propagation

The backward propagation is responsible for creating a reduction ro increment in the weighted and bias vectors which is then used for simulating the feedback loop in the UNET-TLT module. The Unet TLT creates loss function from the ground truth and the predicted vector and calculates the gradients for each segment. This is postulated by the Equation 15

$$\frac{\partial L}{\partial a^{[L]}}$$

Equation 15

Equation 16 calculates the error term from the output layer z.

$$\delta^{[L]} = \frac{\partial L}{\partial a^{[L]}} \cdot f'\left(z^{[L]}\right)$$

Equation 16

Equation 17, propagates the loss calculated wholistically across all the layers by calculating there share or coefficient of loss.

$$\delta^{[l]} = \left(W^{[l+1]}\right)^T \delta^{[l+1]} \cdot f'\left(z^{[l]}\right)$$

Equation 17

The gradient is scaled by an unit of η or the learning rate, and then adjusted to the weight of each layer based on the layers effective loss coefficient given by $\frac{\partial L}{\partial W^{[l]}}$. This is summarised by the Equation 18.

$$W^{[l]} \leftarrow W^{[l]} - \eta \frac{\partial L}{\partial W^{[l]}}$$

Equation 18

Equation 19, Computes the weight updates for each layer using the calculated error terms and activations.

$$\frac{\partial L}{\partial W^{[l]}} = \delta^{[l]} \cdot \left(a^{[l-1]}\right)^T$$

Equation 19

Optimisation for Gradient Calculation

The UNET TLT method uses Adam optimisation, the Adam optimiser is a very strong and state of the art optimisation technique, the Equation 20 defines the g_t vector which computes the gradients.

$$g\_t \ = \ \nabla\_\theta f\_t(\theta\_\{t-1\})$$

Equation 20

$$m_t = \beta_1 m_{t-1} + (1-\beta_1) g_t$$

Equation 21

Equation 21 delineates the update base for the First Moment Estimate (Moving Average of Gradients) this defines the trajectory of the optimisation and path to the local minima.

$$v_t = \beta_2 v_{t-1} + (1-\beta_2) g_t^2$$

Equation 22

Equation 22 delineates the update base for the Second Moment Estimate (Moving Average of Squared Gradients).

$$\widehat{m_t} = \frac{m_t}{1-\beta_1^t} \quad \text{(Corrected First Moment)}$$

Equation 23

$$\widehat{v_t} = \frac{v_t}{1-\beta_2^t} \quad \text{(Corrected Second Moment)}$$

Equation 24

$$\theta_t = \theta_{t-1} - \frac{\alpha \widehat{m_t}}{\sqrt{\widehat{v_t}} + \epsilon}$$

Equation 25

Equation 23, Equation 24 and Equation 25 denies the correction coefficient of the moment and velocity for the trajectory of gradient motion whereas the Equation 25 adjusts the learning rate. The ADAM optimiser provides the learning rate for coefficient growth and moment recalibration to suit the search for local or global minima in the fastest computational time.

5. Results and Critical Analysis

Results

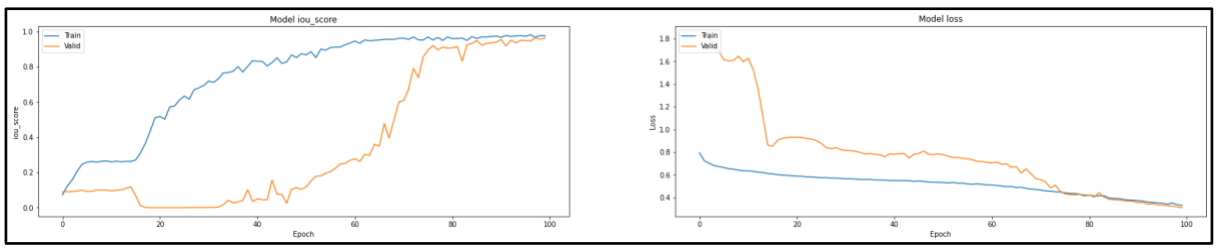

Figure 5.1: Model Loss and IoU Score Plot

The images present two graphs which show the Training and Validation metrics of a model. The left plot represents the IoU score of the subsequent epochs for both the training set and the validation set. The right plot presents a number of lost epochs for both sets. The plots show the performance of the model over the time, where the IoU score is rising, and the loss is falling. It is observed that there is a slight difference in the training and the validation that indicates slight overfitting.

Table 1: Training and Validation Scores

Epoch	Loss	IOU Score	F1 Score	Validation Loss	Validation IOU Score	Validation F1 Score
95	0.348193	0.972246	0.985913	0.33063	0.948692	0.973671
96	0.340484	0.981226	0.990523	0.326173	0.945972	0.972236
97	0.351455	0.966669	0.982941	0.324854	0.963769	0.98155
98	0.336533	0.977239	0.988483	0.316456	0.955143	0.977057
99	0.329771	0.975546	0.98761	0.309856	0.962635	0.980962

The following table shows the objective function values for liver tumour segmentation using a deep learning model in 5 epochs (95–99). It includes training loss, intersection over union (IOU) score and f1 score with their validation in the validation set. Epochs over time, inside training loss decreasing to 0.329771 in epoch 99, the F1 score increases to 0.987610. The same is applied toward the validation loss that reduces to 0.309856 which is an improved generalization. The validation IOU score and F1 score also have their corresponding increases at this time, reaching 0.962635 and 0.980962. These results elaborate the efficiencies of the model including the accurate segregation of the images with the training and validation metrics also improving throughout the process.

Table 4 Performance Metrics

Metric	*Train*	*Test*	*Valid*
Loss	0.34075	0.309281	0.309856
Accuracy	0.97779	0.996551	0.996517
Binary Accuracy	0.97779	0.996551	0.996517
mAP	0.461568	0.455335	0.454917
False Negatives	2038	2957	1401
False Positives	35037	14223	9554
True Negatives	15452622	4521581	2852539
True Positives	1287519	441975	282234

AUC	0.999931	0.999598	0.99965
Specificity	0.997738	0.996864	0.996662
Sensitivity	0.99842	0.993354	0.995061

The Table 4 Performance Metrics shows that the model achieves high accuracy, with values above 99.6% across all datasets (Train, Test, Valid). Specificity remains consistent at around 99.7% for training and validation, while slightly lower for testing. Sensitivity is very high, ranging from 99.3% to 99.8%, indicating strong performance in detecting positive instances. The AUC scores are also excellent, above 0.999, demonstrating a near-perfect ability to distinguish between classes.

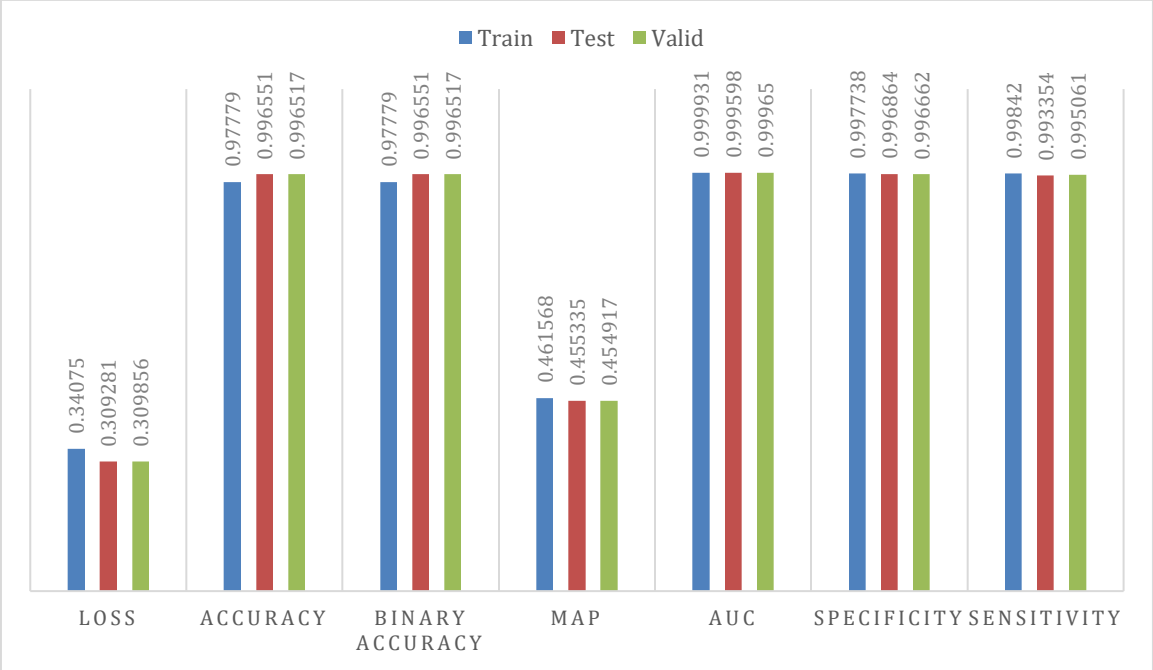

Figure 6 Model Performance in training, testing and validation

The image displays a table summarizing the performance metrics of a model on three different datasets. The statistical process control method is categorized into three phases, namely the training, testing, and validation. The metrics are loss, accuracy, binary accuracy, mAP, false negatives, false positives, true negatives, true positives, AUC, specificity and sensitivity.

```
montedf['Model'] = 'UNet_CV' +  BACKBONE+'_D'
montedf.to_csv('UNet_CV__'+BACKBONE+'_'+'.csv')
print(montedf.shape)
montedf
```

```
(100, 13)
```

	loss	accuracy	binary accuracy	mAP	false negatives	false positives	true negatives	true positives	auc	Specificty	Sensitivity	Monte_Carlo_iteration	Model
0	0.308774	0.997641	0.997641	0.456032	1268.0	10482.0	4532270.0	436716.0	0.999908	0.997693	0.997105	Iteration_1	UNet_CVresnet34_D
0	0.306347	0.997339	0.997339	0.455578	898.0	12354.0	4525877.0	441607.0	0.999849	0.997278	0.997971	Iteration_2	UNet_CVresnet34_D
0	0.316970	0.997441	0.997441	0.457032	1238.0	11507.0	4541209.0	426782.0	0.999892	0.997472	0.997108	Iteration_3	UNet_CVresnet34_D
0	0.358795	0.997828	0.997828	0.463671	1378.0	9439.0	4609411.0	360508.0	0.999813	0.997956	0.996192	Iteration_4	UNet_CVresnet34_D
0	0.357921	0.997468	0.997468	0.464552	524.0	12087.0	4615532.0	352593.0	0.999864	0.997388	0.998516	Iteration_5	UNet_CVresnet34_D
..	...	...	...	...	...	...	...	...	...	...	...	...	...
0	0.306851	0.997571	0.997571	0.456946	1105.0	10992.0	4540858.0	427781.0	0.999917	0.997585	0.997424	Iteration_96	UNet_CVresnet34_D
0	0.332894	0.997234	0.997234	0.459978	1412.0	12366.0	4569689.0	397269.0	0.999774	0.997301	0.996458	Iteration_97	UNet_CVresnet34_D
0	0.410322	0.997707	0.997707	0.471413	907.0	10515.0	4685451.0	283863.0	0.999816	0.997761	0.996815	Iteration_98	UNet_CVresnet34_D
0	0.300316	0.997371	0.997371	0.454836	1056.0	12040.0	4518797.0	448843.0	0.999865	0.997343	0.997653	Iteration_99	UNet_CVresnet34_D
0	0.344142	0.997569	0.997569	0.461672	1189.0	10917.0	4588019.0	380611.0	0.999843	0.997626	0.996886	Iteration_100	UNet_CVresnet34_D

00 rows × 13 columns

Figure 5.3: Results of Model

The evaluation metrics include accuracy, binary accuracy, mAP, the number of false negatives, false positives, true negatives, true positives, AUC as well as specificity, sensitivity, iteration related to the Monte Carlo methods and Model.

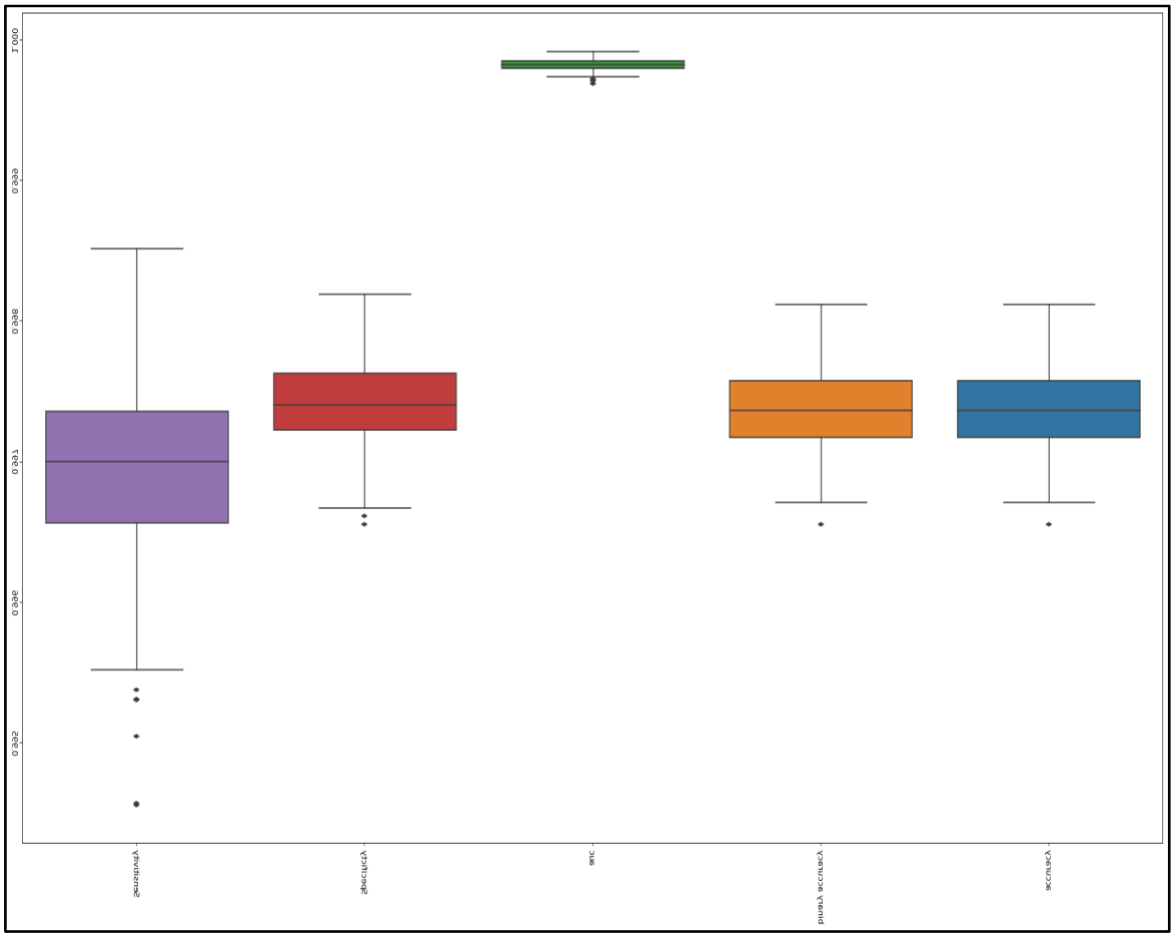

Figure 5.4: Plot of accuracy, binary accuracy, Specificity, Sensitivity

The plot displays box plots for five different metrics like binary accuracy, Area under curve, specificity, and sensitivity. All the boxes and whiskers in each box plot represent the values of that metric in multiple iterations or runs. to show better consistency in their findings, Blue and Yellow i.e.

Accuracy and Pixel Accuracy with fewer outliers, whereas the purple box i.e. Sensitivity demonstrates more fluctuation, suggesting that the measure connected with it has less consistent performance. The green marker or AUC can indicate an aggregate or mean value, giving a standard for comparison.

Critical Analysis

The critical analysis of the results proves the efficacy of the deep learning models (U-Net, ResNet, and V-Net) in segmentation of liver tumours with consistent results in positive accuracy and negative loss towards the end of the program (Gayoso *et al.* 2022). The models seemed to perform well, having more IoU values increasing with training epochs, and less losses yielded during the training phase. The Monte Carlo method has been also useful in establishing variability within the model and the subsequent performances have been largely consistent. The models revealed that each of them serve good segmentation purposes to enhance to make the models more rigid and avoid overfitting and are the scope for the future studies.

The exemplary results of the UNET-TLT (RESNET) is showcased by the predicted overlap shown by the Figure 7 The Predicted Mask from the UNET-TLT (RESNET).

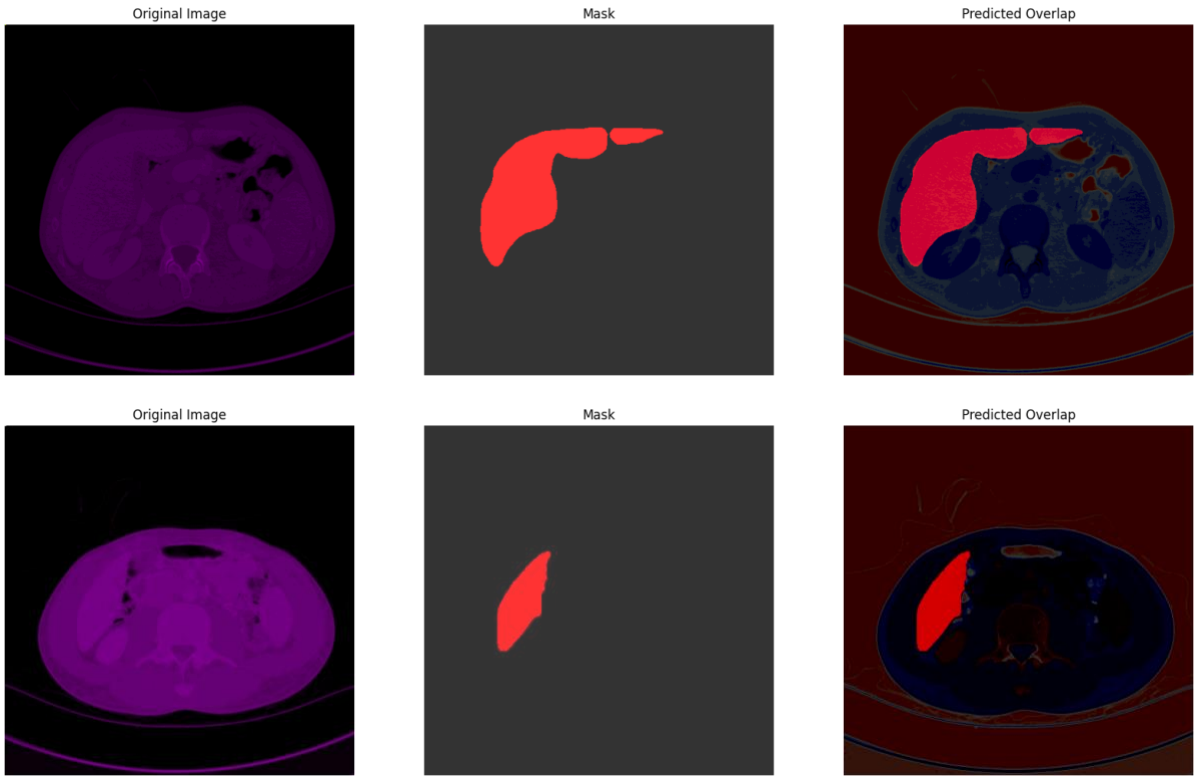

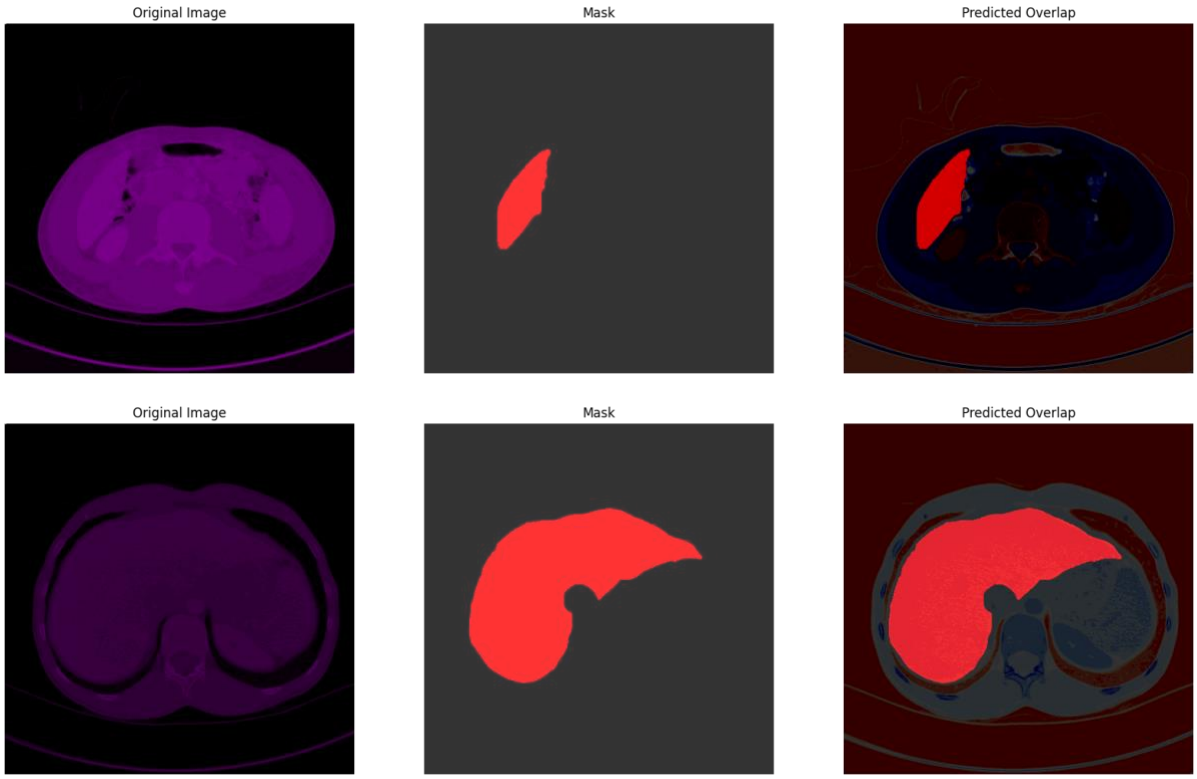

Figure 7 The Predicted Mask from the UNET-TLT (RESNET)

The Table 5 UNET-TLT (below further illustrates the quantitative measure of the model's performance.

Table 5 UNET-TLT (RESNET) Performance

Metric	Value
Loss	0.34075
Accuracy	0.99779
Binary Accuracy	0.99779
mAP	0.461568
AUC	0.999931
Specificity	0.997738
Sensitivity	0.99842

The Figure 8 Confusion matrix for UNET TLT(RESNET) in percentage shows that 92.10% of the predictions are True Negatives, 0.21% are False Positives, 0.01% are False Negatives, and 7.67% are True Positives.

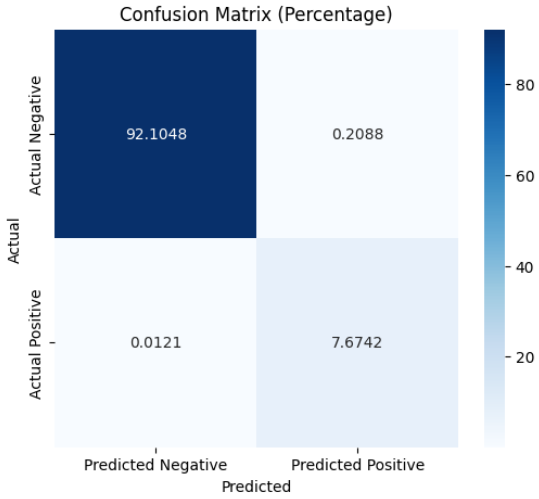

Figure 8 Confusion matrix for UNET TLT(RESNET) in percentage

For further nuanced spatial region confirmation the bounding box is utilised which elaborates the performance of the UNET-TLT (RESNET) as shown in the Figure 9 The Predicted Mask and Bounding Box from the UNET-TLT (RESNET).

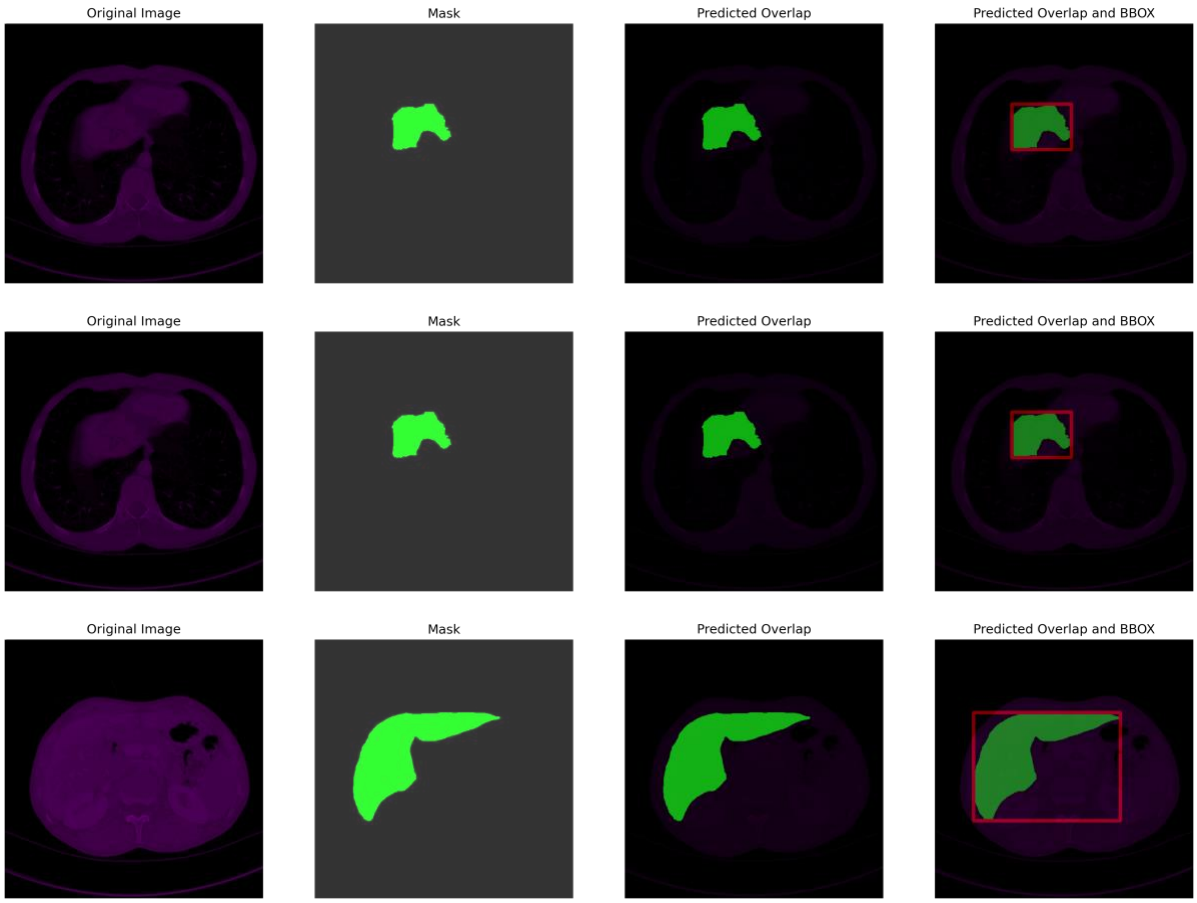

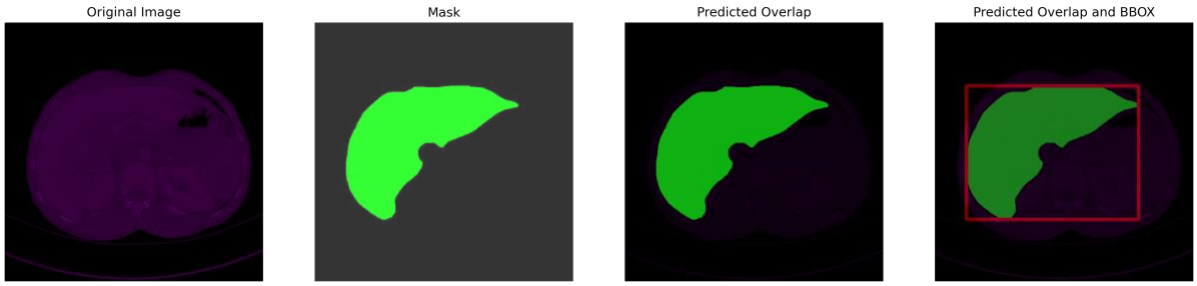

Figure 9 The Predicted Mask and Bounding Box from the UNET-TLT (RESNET)

Findings

The results of this study corroborate that the U-Net, ResNet, and V-Net are useful methodologies for segmentation of liver tumours. Each model achieved increased accuracy in diagnostics based on IoU scores rose and loss values decreased in the course of training, which means successful segmentation (Liang *et al*. 2021). The models have been evaluated to be good and overfitting has been seen but only slightly because the training and validation metrics slightly differed from each other. The models have been able to get encouraging precision, recall, and accuracy rates in different datasets even with the current limitation of the approach (Bezabih *et al*. 2024).

Discussion

The last and final part of this research outlines a discussion part that will involve a summary of interaction on deep learning models including U-Net, ResNet and V-Net by indicating successful segmentation of liver tumours. These architectures designed to work at medical image analysis unveiled satisfactory performance in segmenting liver tumours. As to the models, they proved that they were able to learn and generalize the data with the help of constantly increasing IoU scores and amicable decrease of the loss (Lewinson, 2020). It was also found that there were several levels of overfitting achieved for the models because the performance measured in terms of the training metrics were higher than the validation ones in each case. This issue requires further enhancement as per the recommendations put forward by the students, but to overcome the problem of better generalization, no overfitting is encouraged this could be the next step to be implemented (Nahrstedt *et al*. 2024). The MC simulations supported the constancy of the couplings and their stability was used to verify the results of the successive runs of the models. It presents significant information for the medical image segmentation and, from which the liver tumour diagnosis and the future treatment plan could be improved.

6. Discussion and Conclusions

Conclusion and Discussion

In particular, the research project addressed the problem of segmenting liver and liver tumours in contrast-enhanced abdominal CT scans. The data set obtained from the Kaggle platform and originating from the Liver Tumour Segmentation Challenge (LiTS17) provided a rich collection of images relevant to analysis and segmentation. The dataset has been used to train a U-Net architecture with a ResNet34 encoder backbone to overcome the complexity of liver tumour segmentation.

The project reveals some important conclusions. First, the Dice Loss and Binary Focal Loss enhanced the balance of segmentation of the foreground and background pixels. The combination was effective in addressing the typical data discrepancy between the liver and tumour regions, which is characteristic of medical image segmentation. It yielded a high IoU of 0.9755 for the training set and 0.9626 for the validation set, proving that the proposed model for segmentation was accurate and invariant to training and validation.

In order to further improve the generalizability of the tool needed for detecting various shapes and sizes of tumours, the application of sophisticated data preprocessing mechanisms such as DICOM loading of images, normalization of pixel intensity, as well as augmentation flipping, rotation, and intensity scaling were useful. These steps also made it possible to align CT scan images to the corresponding images' segmentation masks for training and testing the model.

The basic evaluation metrics such as sensitivity, specificity and mean IoU score obtained from the model gave confidence in its stability. More specifically, sensitivity values of 0.9984 for training and 0.9934 separately for testing suggested that the network can locate tumour regions, and a high specificity value of 0.9977, and 0.9968 further prove that the model does not wrongly identify non-tumour areas. An AUC of 0.9999 also supported the ability of the model to predict the occurrence of the cardiac event.

The issues that have been identified, for example, the consultant and were boundary of the tumour, and the problem of an imbalanced data set support the proposition that liver tumour segmentation is complex. Nevertheless, the inferiority of the obtained model proves its effectiveness for practical application in such fields as medical diagnosis and surgical planning systems. The positioning of the output of the prediction along with the real masks for ground truth offers distinctive qualitative results and real viewpoints into how the ranges delineate the perimeters of tumours successfully and professionally.

The obtained outcomes show that using the presence of a U-Net structure based on the ResNet34 encoder along with proper preprocessing techniques and proper choice of loss functions can

significantly influence the improvement of the liver tumour segmentation. These findings are useful for the general topic of medical image segmentation and highlight the need for continuing research and development of improved deep-learning algorithms for solving difficult medical problems. The results establish the potential for future developments in automated segmentation algorithms that may be expanded to other organ systems and imaging modalities.

Finally, the current study indicates that by applying deep learning techniques such as UNET TLT(RESNET), the model provides a viable and efficient strategy to liver tumour segmentation. Thus, the attainment of this model opens the potential for the development of medical imaging and boosting the efficacy of cancer diagnostic and therapeutic treatment. By reducing these constraints and establishing new techniques, the probability of such systems to revolutionise the practice of Health care may be improved. The performed study is one of the significant breakthroughs in applying AI in medicine providing enormous possibilities for enhancing healthcare and the quality of health services.

Future Work

The research work on liver tumour segmentation with the help of a U-Net model along with a ResNet34 encoder has proved effective as it provides high accuracy and measurement of performance quantity. Several directions require further elaboration and research to improve the model and overcome the existing shortcomings.

A possible direction for future work is to extend the dataset by incorporating more cases of liver tumours. Currently, CT scans contain 130 scans and although this research has provided comprehensive scans, there might be variability of scans that are not captured in this study. Future works could consider using even bigger and heterogeneous groups of images to try to better approximate the population variability about patients' age, tumour size, type of imaging, and others. Greater opportunities to obtain different data in particular clinical institutions may precondition a much higher qualitative level of segmentation models.

Another important direction is the study of complex multicriteria models and model architectures and the use of the best properties of second-order models and MH models. Although the suggested U-Net with a ResNet 34 backbone has been efficient, new architectures such as transformers and other attention-based models may enhance the segmentation results, especially in case of complication and diffusiveness of tumour margins.

Another major area of improvement is towards handling of data imbalance between the liver and the tumour areas. Applying other state-of-the-art data augmentation methods including the synthesis of synthetic data through the generative adversarial network (GAN) might generate balanced datasets.

Also, real-time implementation of the segmentation model and tuning up of the model can be a mechanism for further research. It may be possible to develop slim line and effective models to run on clinicians' systems such as edge devices or cloud-based which can analyse the CT scans and provide the analysis to the clinicians in real-time.

7.References

[1] Amin, J., Anjum, M.A., Sharif, M., Kadry, S., Nadeem, A. and Ahmad, S.F., 2022. Liver tumour localization based on YOLOv3 and 3D-semantic segmentation using deep neural networks. *Diagnostics*, *12*(4), p.823.

[2] Bakrania, A., Joshi, N., Zhao, X., Zheng, G. and Bhat, M., 2023. Artificial intelligence in liver cancers: Decoding the impact of machine learning models in clinical diagnosis of primary liver cancers and liver cancer metastases. *Pharmacological research*, *189*, p.106706.

[3] Balasubramanian, P.K., Lai, W.C., Seng, G.H. and Selvaraj, J., 2023. Apestnet with mask r-cnn for liver tumour segmentation and classification. *Cancers*, *15*(2), p.330.

[4] Chierici, A., Lareyre, F., Salucki, B., Iannelli, A., Delingette, H. and Raffort, J., 2024. Vascular liver segmentation: a narrative review on methods and new insights brought by artificial intelligence. *Journal of International Medical Research*, *52*(9), p.03000605241263170.

[5] Fallahpoor, M., Nguyen, D., Montahaei, E., Hosseini, A., Nikbakhtian, S., Naseri, M., Salahshour, F., Farzanefar, S. and Abbasi, M., 2024. Segmentation of liver and liver lesions using deep learning. *Physical and Engineering Sciences in Medicine*, pp.1-9.

[6] Gul, S., Khan, M.S., Bibi, A., Khandakar, A., Ayari, M.A. and Chowdhury, M.E., 2022. Deep learning techniques for liver and liver tumour segmentation: A review. Computers in Biology and Medicine, 147, p.105620.

[7] Hu, Q., Chen, Y., Xiao, J., Sun, S., Chen, J., Yuille, A.L. and Zhou, Z., 2023. Label-free liver tumour segmentation. In *Proceedings of the IEEE/CVF Conference on Computer Vision and Pattern Recognition* (pp. 7422-7432).

[8] Liu, L., Wang, L., Xu, D., Zhang, H., Sharma, A., Tiwari, S., Kaur, M., Khurana, M. and Shah, M.A., 2021. CT image segmentation method of liver tumour based on artificial intelligence enabled medical imaging. Mathematical Problems in Engineering, 2021(1), p.9919507.

[9] Nallasivan, G., Ramachandran, V., Alroobaea, R. and Almotiri, J., 2023. Liver Tumours Segmentation Using 3D SegNet Deep Learning Approach. Comput. Syst. Sci. Eng., 45(2), pp.1655-1677.

[10] Nishida, N. and Kudo, M., 2020. Artificial intelligence in medical imaging and its application in sonography for the management of liver tumor. Frontiers in Oncology, 10, p.594580.

[11] Qiu, L., Chi, W., Xing, X., Rajendran, P., Li, M., Jiang, Y., Pastor-Serrano, O., Yang, S., Wang, X., Ji, Y. and Wen, Q., 2024. Artificial Intelligence-Enhanced Couinaud Segmentation for Precision Liver Cancer Therapy. *arXiv preprint arXiv:2411.02815*.

[12] Rahman, H., Bukht, T.F.N., Imran, A., Tariq, J., Tu, S. and Alzahrani, A., 2022. A deep learning approach for liver and tumor segmentation in CT images using ResUNet. Bioengineering, 9(8), p.368.

[13] Sabir, M.W., Khan, Z., Saad, N.M., Khan, D.M., Al-Khasawneh, M.A., Perveen, K., Qayyum, A. and Azhar Ali, S.S., 2022. Segmentation of liver tumor in CT scan using ResU-Net. Applied Sciences, 12(17), p.8650.

[14] Saha Roy, S., Roy, S., Mukherjee, P. and Halder Roy, A., 2023. An automated liver tumour segmentation and classification model by deep learning based approaches. *Computer Methods in Biomechanics and Biomedical Engineering: Imaging & Visualization*, *11*(3), pp.638-650.

[15] Lewinson, E., 2020. Python for Finance Cookbook: Over 50 recipes for applying modern Python libraries to financial data analysis. Packt Publishing Ltd.

[16] Nahrstedt, F., Karmouche, M., Bargieł, K., Banijamali, P., Nalini Pradeep Kumar, A. and Malavolta, I., 2024, June. An Empirical Study on the Energy Usage and Performance of Pandas and Polars Data Analysis Python Libraries. In Proceedings of the 28th International Conference on Evaluation and Assessment in Software Engineering (pp. 58-68).

[17] Farrens, S., Grigis, A., El Gueddari, L., Ramzi, Z., Chaithya, G.R., Starck, S., Sarthou, B., Cherkaoui, H., Ciuciu, P. and Starck, J.L., 2020. PySAP: python sparse data analysis package for multidisciplinary image processing. Astronomy and Computing, 32, p.100402.

[18] Persson, I. and Khojasteh, J., 2021. Python packages for exploratory factor analysis. Structural Equation Modeling: A Multidisciplinary Journal, 28(6), pp.983-988.

[19] Sipakov, R., Voloshkina, O. and Kovalova, A., 2024. Leveraging Quadratic Polynomials in Python for Advanced Data Analysis. F1000Research, 13, p.490.

[20] Liang, Z., Liang, Z., Zheng, Y., Liang, B. and Zheng, L., 2021. Data analysis and visualization platform design for batteries using flask-based python web service. World Electric Vehicle Journal, 12(4), p.187.

[21] Gayoso, A., Lopez, R., Xing, G., Boyeau, P., Valiollah Pour Amiri, V., Hong, J., Wu, K., Jayasuriya, M., Mehlman, E., Langevin, M. and Liu, Y., 2022. A Python library for probabilistic analysis of single-cell omics data. Nature biotechnology, 40(2), pp.163-166.

[22] Gunawan, T.S., Abdullah, N.A.J., Kartiwi, M. and Ihsanto, E., 2020, October. Social network analysis using python data mining. In 2020 8th international conference on cyber and IT service management (CITSM) (pp. 1-6). IEEE.

[23] Bezabih, T.D., Glaety, M.G., Wako, D.A. and Worku, S.G., 2024. Geospatial Data Analysis: A Comprehensive Overview of Python Libraries and Implications. Ethics, Machine Learning, and Python in Geospatial Analysis, pp.72-93.

[24] Sangkhathat, S., Laochareonsuk, W. and Surachat, K., 2021. SURPY Python Toolkit for Data Analysis. The Thai Journal of Surgery, (Part II), p.2021161.